On Scattering in a Piezoelectric Medium by a Conducting Crack

Shaofan Li[1]
e-mail: li@ce.Berkeley.edu

Albert C. To

Steven D. Glaser

Department of Civil and Environmental Engineering,
University of California,
Berkeley, CA 94720

The work is concerned with the characterization of a Kirchhoff diffraction field in a piezoelectric material. An exact solution is obtained for the full scattering fields around the tip of a semi-infinite crack, which is electrically conducting and is loaded with both SH acoustic incident waves and in-plane electrical incident waves. First, it is found that a conducting crack in a piezoelectric solid is not completely opaque to the electro-acoustic wave, i.e., the electro-acoustic wave can penetrate and transmit to the other side of the crack surface. Second, the analysis has confirmed that the interaction between electrical wave and acoustic wave will provide multiple electrical and electro-acoustic head waves. Third, by solving the problem, we have established a rigorous electro-acoustic scattering theory in piezoelectric/ferroelectric media, which is different from the scattering theory in purely elastic media. The characterization of the scattering fields in piezoelectric media provides a unique signature database for electro-acoustic waves in piezoelectric materials. [DOI: 10.1115/1.2047627]

1 Introduction

Wave scattering theory in piezoelectric/ferroelectric materials has been an important research area for many years (e.g., [1]), and it is the very foundation of sensor technology because piezoelectric/ferroelectric ceramics and thin films are extensively used in the design of various sensors, transducers, and actuators (e.g., [2–6] and many others).

These devices are widely used in various micro-electro-mechanical systems, which include acoustic devices, optical wave devices and surface wave devices (SAW), integrated circuits, and random access memories. Nevertheless, traditional scattering theory has been mainly focused on electric wave scattering without considering electro-acoustic coupling effects. Recently, there are interests in studies on scattering of electro-acoustic waves by defects in piezoelectric/ferroelectric media, e.g., [7,8].

In fact, electro-acoustic wave scattering phenomena in sensors and thin films may be more important than purely electric wave scattering, because it is not only pertinent to the performance of the devices but also nondestructive evaluation of such devices (e.g., [9]). Surprisingly, the scattering theory of electro-acoustic waves in piezoelectric materials has rarely been studied, and it remains an open research subject. A lesser-known reason attributed to the fact is that the initial boundary value problem of the fully coupled Maxwell-Christoffel equations in piezoelectric materials are too complicated to solve, and the simplified wave equations under quasi-static approximation are not mathematically well-posed (see [10,11]). This theoretical inadequacy has, at least partly, attributed to the lack of understanding in electro-acoustic wave scattering theory.

To regularize wave equations in piezoelectric media while still retaining the simplicity of the quasi-static approximation, a few regularization procedures have been proposed recently. We would like to mention the contribution made by Li [12,13] and Daros [14]. Recent developments intend to provide a theoretical ground to establish a rigorous electro-acoustic wave scattering theory for piezoelectric materials. The first systematic effort of establishing an electro-acoustic scattering wave theory in piezoelectric materials has been performed in [15]. However, the solution obtained in [15] is limited by a special assumption that the electric potential in front of the crack tip is zero, which may not be valid in general cases. Moreover, the scattering fields due to an electric source have not been discussed [15].

The objective of this work is to establish a rigorous theory for electro-acoustic wave scattering in piezoelectric materials. In this work, we revisit the electro-acoustic wave scattering theory of piezoelectric materials. In specific, we shall seek to characterize the scattering fields generated by a conducting anti-plane crack (mode III) in a piezoelectric material, which is subjected to both plane SH incident acoustic waves and plane electrical incident waves. Using the standard terminology in wave mechanics, we are seeking the solution for a benchmark problem of wave mechanics in a piezoelectric medium, i.e., Kirchhoff diffraction in a piezoelectric medium. *It should be noted that although the analysis of electro-acoustic scatterings by a mode III crack may be simpler than that of in-plane crack, it does provide the essential characters for the in-plane crack scattering phenomena as well.*

The motivation for doing so is twofold: (1) the Kirchhoff diffraction is often used to describe a (scalar) wave scattering field due to a monochromatic line or point source in the presence of an "opaque" (e.g., electrically conducting) screen. Despite skepticism that the model lacks "physical ground," the solution of a Kirchhoff field in a piezoelectric medium is an exact solution to the coupled wave equations, which *exactly obeys definite, though unusual, boundary conditions [16,17]*, and hence it will become an essential part of the theoretical foundation for other scattering problems from screens that have general impedance properties; (2) For many sensors and transducers, electric loading is applied by using thin electrode layers attached on a surface or embedded in an interface of a piezoelectric block or between ferroelectric thin films. Thus, discontinuous electrode layers are widely used in various layered devices in order to fulfill the designed purposes. *Recently, interfacial fracture between embedded electrode layers and ceramic layers has been identified as a major failure mode in sensors (e.g., by Suo [18,19] and Ru [20]).* For more background information, readers may consult works by Ru et al. [21,20], Winzer et al. [22], Furuta and Uchino [23] Aburatani et al. [24], Freiman and White [25], Hao et al. [26], and Uchino [6].

It may be more practical to find a scattering field by a permeable or an impermeable crack (e.g., [27–29]). Nonetheless, it is the opinion of the authors that a sensible and an appropriate de-

[1]To whom correspondence should be addressed.

Contributed by the Applied Mechanics Division of THE AMERICAN SOCIETY OF MECHANICAL ENGINEERS for publication in the ASME JOURNAL OF APPLIED MECHANICS. Manuscript received by the Applied Mechanics Division December 25, 2004; final revision April 9, 2005. Review conducted by Z. Suo. Discussion on the paper should be addressed to the Editor, Prof. Robert M. McMeeking, Journal of Applied Mechanics, Department of Mechanical and Environmental Engineering, University of California—Santa Barbara, Santa Barbara, CA 93106-5070, and will be accepted until four months after final publication in the paper itself in the ASME JOURNAL OF APPLIED MECHANICS.

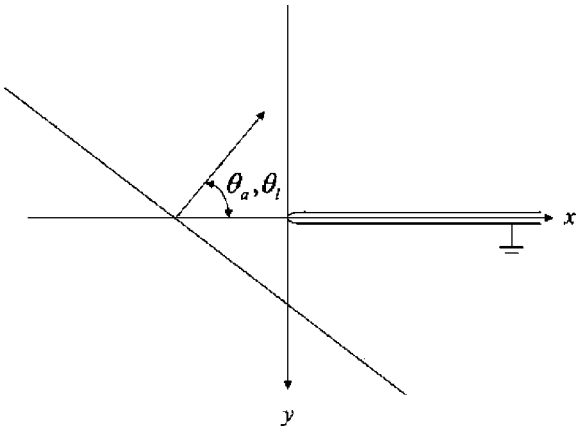

Fig. 1 Schematic illustration of a system of plane waves due to an incident acoustic wave approaching a semi-infinite crack

parture point for establishing a rigorous electro-acoustic wave scattering theory in piezoelectric media is to first study the Kirchhoff diffraction of electro-acoustic waves.

The presentation of the paper is organized in six sections: The initial boundary value problem of the scattering problem is set in Sec. 2. In Sec. 3, the main procedure solution is discussed; Sec. 4 provides a full characterization of the scattering fields in front of the crack tip, and in Sec. 5, the features of the scattering fields are discussed in details. At last, a few concluding remarks are made in Sec. 6.

2 The Scattering Problem

2.1 Formulation. Consider a transversely isotropic piezoelectric space that contains a semi-infinite slit, which lies at $y=0$ and $x \geqslant 0$ with respect to a Cartesian coordinate system (x,y,z) shown in Fig. 1. It is assumed that the interface slit is mechanically stress free and short circuited and has a vanishingly small thickness.

For the diffraction problem considered in this paper, the relevant electromechanical coupling on the transverse plane is between anti-plane displacement and in-plane electric field,

$$\mathbf{u} = (0,0,w(x,y,t)) \tag{1}$$

$$\mathbf{E} = \left(-\frac{\partial \phi}{\partial x}, -\frac{\partial \phi}{\partial y}, 0\right). \tag{2}$$

Following [12], we introduce a pseudo-electric wave potential function

$$\psi = \phi - \frac{e_{15}}{\epsilon_{11}} C_f w \tag{3}$$

where $C_f := c_\ell^2/(c_\ell^2 - c_a^2)$, e_{15} is the piezoelectric stress constant, and ϵ_{11} is the specific dielectric constant. $c_\ell := (\epsilon_{11}\mu_0)^{-1/2}$ is the speed of light and $c_a := \sqrt{\bar{c}_{44}/\rho}$ is the acoustic speed, where $\bar{c}_{44} := c_{44}^E + e_{15}^2/\epsilon_{11}$, μ_0 is the magnetic permeability constant in vacuum, and c_{44}^E is the purely elastic shear modulus in the transverse direction.

Based on the "quasi-hyperbolic approximation" introduced by Li [15], we can then derive a set of decoupled wave equations,

$$\left(\frac{\partial^2}{\partial x^2} + \frac{\partial^2}{\partial y^2} - \frac{1}{c_a^2}\frac{\partial^2}{\partial t^2}\right) w = 0 \tag{4}$$

$$\left(\frac{\partial^2}{\partial x^2} + \frac{\partial^2}{\partial y^2} - \frac{1}{c_\ell^2}\frac{\partial^2}{\partial t^2}\right) \psi = 0. \tag{5}$$

Under the quasi-hyperbolic approximation, the relevant constitutive equations are

$$\sigma_{xz} = \tilde{c}_{44}\frac{\partial w}{\partial x} + e_{15}\frac{\partial \psi}{\partial x} \tag{6}$$

$$\sigma_{yz} = \tilde{c}_{44}\frac{\partial w}{\partial y} + e_{15}\frac{\partial \psi}{\partial y} \tag{7}$$

$$D_x = e_{15}(1 - C_f)\frac{\partial w}{\partial x} - \epsilon_{11}\frac{\partial \psi}{\partial x}. \tag{8}$$

$$D_y = e_{15}(1 - C_f)\frac{\partial w}{\partial y} - \epsilon_{11}\frac{\partial \psi}{\partial y} \tag{9}$$

where $\tilde{c}_{44} := \bar{c}_{44}[1-(1-C_f)(e_{15}^2/\bar{c}_{44}\epsilon_{11})]$.

2.2 The Scattering Problem. For time $t<0$, an incident SH acoustic plane wave or an incident pseudo-electric wave propagates from afar toward the semi-infinite slit. The incident plane waves are assumed to have the following form:

$$w^{(i)}(x,y,t) = w_0^{(i)} G(t - s_a[\cos(\theta_a)x - \sin(\theta_a)y]) \tag{10}$$

$$\psi^{(i)}(x,y,t) = \psi_0^{(i)} G(t - s_\ell[\cos(\theta_\ell)x - \sin(\theta_\ell)y]) \tag{11}$$

where the subscripts "a" and "ℓ" correspond to the acoustic and pseudo-electric waves. $w_0^{(i)}$ and $\psi_0^{(i)}$ are the respective plane wave amplitudes and $s_a := 1/c_a$ and $s_\ell := 1/c_\ell$ are the respective slownesses. $0 \leqslant \theta_a, \theta_\ell \leqslant \pi/2$ are angles of incident waves. The shape function $G(\cdot)$ is a real-valued function defined to be

$$G(t) := H(t)\int_0^t g(\tau)d\tau \tag{12}$$

where $g(\cdot)$ is a given real value function, and $H(t)$ is the Heaviside function. For simplicity, it is assumed that both the incident acoustic and pseudo-electric waves have the same shape functions. In the case that they are different, superposition can be used to obtain the solution due to linearity of the problem.

Although the material properties in the upper and lower half spaces are identical, it may be more convenient to treat them separately for the time being. The field variables in the upper half space ($y \leqslant 0$) and in the lower half space ($y>0$) are labeled by the superscripts u and l, respectively. At time $t=0$, the incident plane wave arrives at the crack tip and is being scattered. The total solutions of the scattering problem are

$$w(x,y,t) = w^{(i)}(x,y,t) + w^{(s)}(x,y,t), \tag{13}$$

$$\psi(x,y,t) = \psi^{(i)}(x,y,t) + \psi^{(s)}(x,y,t). \tag{14}$$

The superscript "(i)" indicates the incident field and "(s)" indicates the scattering field.

For a conducting crack, the crack surface is traction-free and electrically grounded,

$$\sigma_{yz}^u(x,0,t) = \sigma_{yz}^l(x,0,t) = 0, \quad x \geqslant 0 \tag{15}$$

$$\phi^u(x,0,t) = \phi^l(x,0,t) = 0, \quad x \geqslant 0 \tag{16}$$

and ahead of the crack tip both mechanical and electrical displacements are continuous,

$$w^u(x,0,t) = w^l(x,0,t), \quad x < 0 \tag{17}$$

$$D_y^u(x,0,t) = D_y^l(x,0,t), \quad x < 0. \tag{18}$$

Consideration of Eqs. (13)–(18) leads to the following set of boundary conditions for the scattered waves:

$$\sigma_{yz}^{u(s)}(x,0,t) = \sigma_{yz}^{l(s)}(x,0,t) = -\sigma_{yz}^{(i)}(x,0,t), \quad x \geqslant 0 \tag{19}$$

$$\phi^{u(s)}(x,0,t) = \phi^{l(s)}(x,0,t) = -\phi^{(i)}(x,0,t), \quad -x > 0 \tag{20}$$

$$w^{u(s)}(x,0,t) = w^{l(s)}(x,0,t), \quad x < 0 \tag{21}$$

$$D_y^u(x,0,t) = D_y^l(x,0,t), \quad x < 0. \tag{22}$$

For scattering fields, the following initial conditions and radiation conditions are imposed as

$$w^{(s)}(x,y,t) = \dot{w}^{(s)}(x,y,t) = 0, \quad t < 0 \tag{23}$$

$$\psi^{(s)}(x,y,t) = \dot{\psi}^{(s)}(x,y,t) = 0, \quad t < 0 \tag{24}$$

and

$$\lim_{r\to\infty}(w^{(s)}, \psi^{(s)}, \dot{w}^{(s)}, \dot{\psi}^{(s)}) = 0, \quad t > 0 \tag{25}$$

Since the incident and total displacement fields and pseudo-electric potential obey the wave equations (4) and (5), by virtue of (13) and (14), the scattered displacement field $w^{(s)}$ and the scattered pseudo-electric potential $\psi^{(s)}$ must also obey the same equations. For simplicity, the superscript "(s)" denoting the scattering fields is dropped in the rest of the paper if no confusion may occur.

3 Solution Procedures

3.1 Transform Methods. In this section, the standard procedure of multiple Laplace transforms is employed to seek the solution of the above mixed initial boundary value problem. The multiple transforms are introduced for the variable pair (x,t). To suppress the time variable t, the usual, one-sided Laplace transform is applied:

$$f^*(x,y,p) = \int_0^\infty f(x,y,t)\exp(-pt)dt, \tag{26}$$

$$f(x,y,t) = \frac{1}{2\pi i}\int_{Br_1} f^*(x,y,p)\exp(pt)dp, \tag{27}$$

where the inversion integration is taken over the usual Bromwich path.

To suppress the spatial variable x, the two-sided Laplace transform is used:

$$\hat{f}^*(\zeta,y,p) = \int_{-\infty}^\infty f^*(x,y,p)\exp(-p\zeta x)dx \tag{28}$$

$$f^*(x,y,p) = \frac{p}{2\pi i}\int_{Br_2} \hat{f}^*(\zeta,y,p)\exp(p\zeta x)d\zeta \tag{29}$$

After transformation, the governing equations (4) and (5) for the scattered waves become

$$\left(\frac{d^2}{dy^2} - p^2\alpha^2(\zeta)\right)\hat{w}^*(\zeta,y,p) = 0 \tag{30}$$

$$\left(\frac{d^2}{dy^2} - p^2\beta^2(\zeta^2)\right)\hat{\psi}^*(\zeta,y,p) = 0 \tag{31}$$

where $\alpha(\zeta) := \sqrt{s_a^2 - \zeta^2}$ and $\beta(\zeta) := \sqrt{s_\ell^2 - \zeta^2}$.

To satisfy the boundary conditions at infinity, we choose the solution of the following form:

$$\left.\begin{aligned} \hat{w}^{l*}(\zeta,y,p) &= \frac{1}{p^2}A^l(\zeta)\exp(-p\alpha y) \\ \hat{\psi}^{l*}(\zeta,y,p) &= \frac{1}{p^2}B^l(\zeta)\exp(-p\beta y) \end{aligned}\right\} y > 0, \tag{32}$$

$$\left.\begin{aligned} \hat{w}^{u*}(\zeta,y,p) &= -\frac{1}{p^2}A^u(\zeta)\exp(p\alpha y) \\ \hat{\psi}^{u*}(\zeta,y,p) &= -\frac{1}{p^2}B^u(\zeta)\exp(p\beta y) \end{aligned}\right\} y < 0. \tag{33}$$

In Eqs. (32) and (33), $\mathrm{Re}(\alpha(\zeta),\beta(\zeta)) \geqslant 0$ in the plane with branch cuts:

$$\alpha\text{: } \mathrm{Im}(\zeta) = 0, \quad \mathrm{Re}(\zeta) < -s_a, \quad \text{and} \quad \mathrm{Re}(\zeta) > s_a, \tag{34}$$

$$\beta\text{: } \mathrm{Im}(\zeta) = 0, \quad \mathrm{Re}(\zeta) < -s_\ell, \quad \text{and} \quad \mathrm{Re}(\zeta) > s_\ell. \tag{35}$$

3.2 The Wiener-Hopf Decomposition. A powerful technique to find the solution in transformed space is the Wiener-Hopf decomposition. To apply the Wiener-Hopf technique, it is expedient to expand the mechanical and electrical boundary conditions over the full range of the x axis. This can be done by introducing two unknown functions:

$$\sigma_-(x,t) := \begin{cases} \sigma_{yz}^l(x,0,t) = \sigma_{yz}^u(x,0,t) & x < 0, \\ 0 & x \geqslant 0, \end{cases} \tag{36}$$

$$\phi_-(x,t) := \begin{cases} \phi^l(x,0,t) = \phi^u(x,0,t) & x < 0, \\ 0 & x \geqslant 0, \end{cases} \tag{37}$$

$$\Delta w_+(x,t) := \begin{cases} 0 & x < 0, \\ w^l(x,0,t) - w^u(x,0,t) & x \geqslant 0, \end{cases} \tag{38}$$

$$\Delta D_+(x,t) := \begin{cases} 0 & x < 0, \\ D_y^l(x,0,t) - D_y^u(x,0,t) & x \geqslant 0. \end{cases} \tag{39}$$

so that

$$\sigma_{yz}^l(x,0,t) = \sigma_{yz}^u(x,0,t) = \sigma_-(x,t) - \sigma_{yz}^{(i)}(x,0,t), \quad -\infty < x < \infty \tag{40}$$

$$\phi^l(x,0,t) = \phi^u(x,0,t) = \phi_-(x,t) - \phi^{(i)}(x,0,t), \quad -\infty < x < \infty \tag{41}$$

$$w^l(x,0,t) - w^u(x,0,t) = 0 + \Delta w_+(x,t), \quad -\infty < x < \infty \tag{42}$$

$$D_y^l(x,0,t) - D_y^u(x,0,t) = 0 + \Delta D_+(x,t), \quad -\infty < x < \infty. \tag{43}$$

After suppressing both x and t,

$$\hat{\sigma}_{yz}^{l*}(\zeta,0,p) = \hat{\sigma}_{yz}^{u*}(\zeta,0,p) = \frac{\Sigma_-(\zeta)}{p} - \hat{\sigma}_{yz}^{*(i)}(\zeta,0,p) \tag{44}$$

$$\hat{\phi}^{l*}(\zeta,0,p) = \hat{\phi}^{u*}(\zeta,0,p) = \frac{\Phi_-(\zeta)}{p^2} - \hat{\phi}^{*(i)}(\zeta,0,p) \tag{45}$$

$$\frac{\hat{w}^{l*}(\zeta,0,p) - \hat{w}^{u*}(\zeta,0,p)}{2} = \frac{\Delta U_+(\zeta)}{p^2} \tag{46}$$

$$\frac{\hat{D}_y^{l*}(\zeta,0,p) - \hat{D}_y^{u*}(\zeta,0,p)}{2} = \frac{\Delta D_+(\zeta)}{p} \tag{47}$$

where

$$\Sigma_-(\zeta) := p\int_{-\infty}^0 \sigma_-^*(x,p)\exp(-p\zeta x)dx \tag{48}$$

$$\Phi_-(\zeta) := p^2\int_{-\infty}^0 \phi_-^*(x,p)\exp(-p\zeta x)dx \tag{49}$$

$$\Delta U_+(\zeta) := p^2\int_0^\infty \frac{\Delta w_+^*(x,p)}{2}\exp(-p\zeta x)dx \tag{50}$$

$$\Delta D_+(\zeta) \coloneqq p\int_0^\infty \frac{\Delta D_+^*(x,p)}{2}\exp(-p\zeta x)dx \tag{51}$$

On the other hand, employing the constitutive equations (6)–(9) and substituting the general solutions and (32) and (33) into Eqs. (48)–(51), one may obtain the following sets of equations:

$$\hat{\sigma}_{yz}^{l*} + \hat{\sigma}_{yz}^{u*} \Rightarrow -\hat{c}_{44}\alpha(\zeta)A_{sy}(\zeta) - e_{15}\beta(\zeta)B_{sy}(\zeta) = \Sigma_-(\zeta) - p\hat{\sigma}_{yz}^{*(i)} \tag{52}$$

$$\hat{\phi}^{l*} - \hat{\phi}^{u*} \Rightarrow \frac{e_{15}}{\epsilon_{11}}C_f A_{sy}(\zeta) + B_{sy}(\zeta) = 0 \tag{53}$$

$$\hat{w}^{l*} - \hat{w}^{u*} \Rightarrow A_{sy} = \Delta U_+(\zeta) \tag{54}$$

$$\hat{\phi}^{l*} + \hat{\phi}^{u*} \Rightarrow \frac{e_{15}}{\epsilon_{11}}C_f A_{an}(\zeta) + B_{an}(\zeta) = \Phi_-(\zeta) - p^2\hat{\phi}^{*(i)} \tag{55}$$

$$\hat{\sigma}_{yz}^{l*} - \hat{\sigma}_{yz}^{u*} \Rightarrow -\tilde{c}_{44}\alpha(\zeta)A_{an}(\zeta) - e_{15}\beta(\zeta)B_{an}(\zeta) = 0 \tag{56}$$

$$\hat{D}_y^{l*} - \hat{D}_y^{u*} \Rightarrow -e_{15}(1-C_f)\alpha(\zeta)A_{an}(\zeta) + \epsilon_{11}\beta B_{an}(\zeta) = \Delta D_+(\zeta) \tag{57}$$

where $A_{sy}(\zeta)=[A^l(\zeta)+A^u(\zeta)]/2$, $A_{an}(\zeta)=[A^l(\zeta)-A^u(\zeta)]/2$, $B_{sy}(\zeta)=[B^l(\zeta)+B^u(\zeta)]/2$, and $B_{an}(\zeta)=[B^l(\zeta)-B^u(\zeta)]/2$. Now, from these equations, it becomes obvious that two decoupled Wiener-Hopf equations can be obtained:

$$-BG(\zeta)\Delta U_+(\zeta) = \Sigma_-(\zeta) - p\hat{\sigma}_{yz}^{*(i)}(\zeta,0,p) \tag{58}$$

$$\frac{BG(\zeta)\Delta D_+(\zeta)}{\alpha(\zeta)\beta(\zeta)[e_{15}^2(1-C_f)+\epsilon_{11}\tilde{c}_{44}]} = \Phi_-(\zeta) - p^2\hat{\phi}^{*(i)}(\zeta,0,p) \tag{59}$$

where

$$BG(\zeta) = \tilde{c}_{44}(\alpha(\zeta) - \tilde{k}_e^2\beta(\zeta)) \tag{60}$$

is recognized as the Bleustein-Gulyaev wave function [30,31], and $\tilde{k}_e^2$ is the electro-mechanical coupling coefficient:

$$\tilde{k}_e^2 \coloneqq \frac{e_{15}^2}{\epsilon_{11}\tilde{c}_{44}}C_f. \tag{61}$$

The terms $\hat{\sigma}_{yz}^{*(i)}(\zeta,0,p)$ and $\hat{\phi}^{*(i)}(\zeta,0,p)$ in Eqs. (58) and (59) are dependent on the type of incident waves. Employing the incident acoustic wave field and pseudo-electric wave field in Eqs. (10) and (11) and the constitutive equations for stress and electric potential in (7) and (9), one may obtain the stress and electric potential for an incident wave:

$$\hat{\sigma}_{yz}^{*(i)}(\zeta,0,p) = -\frac{\sigma_0 g^*(p)}{p(\zeta+s_h)} \tag{62}$$

$$\hat{\phi}^{*(i)}(\zeta,0,p) = -\frac{\phi_0 g^*(p)}{p^2(\zeta+s_h)} \tag{63}$$

where

$$\sigma_0 = -\bar{c}_{44}s_a\sin(\theta_a)w_0^{(i)} \tag{64}$$

$$\phi_0 = -\frac{e_{15}}{\epsilon_{11}}C_f w_0^{(i)} \tag{65}$$

$$s_h = s_a\cos(\theta_a) \tag{66}$$

for an incident acoustic wave $w^{(i)}$, whereas for an incident pseudo-electric wave $\psi^{(i)}$,

$$\sigma_0 = -e_{15}s_\ell\sin(\theta_\ell)\psi_0^{(i)} \tag{67}$$

$$\phi_0 = -\psi_0^{(i)} \tag{68}$$

$$s_h = s_\ell\cos(\theta_\ell). \tag{69}$$

For convenience, define the Bleustein-Gulyaev wave velocity and slowness:

$$c_{bg} \coloneqq c_a\sqrt{\tilde{C}_f(1-k_e^4)} \quad \text{and } s_{bg} \coloneqq 1/c_{bg}, \tag{70}$$

where

$$\tilde{C}_f \coloneqq \frac{c_\ell^2}{c_\ell^2 - \tilde{k}_e^4 c_a^2}. \tag{71}$$

The detailed solutions to the two Wiener-Hopf equations (58) and (59) are presented in the Appendix, and the main results are

$$A_{sy}(\zeta) = -\frac{\sigma_0 g^*(p)\sqrt{s_a+\zeta}R_-(-s_h)}{(\zeta+s_h)(s_{bg}+\zeta)D_s\mathcal{T}_+(\zeta)}, \tag{72}$$

$$B_{sy}(\zeta) = \frac{e_{15}C_f\sigma_0 g^*(p)\sqrt{s_a+\zeta}R_-(-s_h)}{\epsilon_{11}(\zeta+s_h)(s_{bg}+\zeta)D_s\mathcal{T}_+(\zeta)}, \tag{73}$$

$$A_{an}(\zeta) = -\frac{\phi_0 g^*(p)\sqrt{s_a+\zeta}\sqrt{s_\ell+\zeta}S_-(-s_h)e_{15}}{\sqrt{s_a-\zeta}(s_{bg}+\zeta)\mathcal{T}_+(\zeta)D_s}, \tag{74}$$

$$B_{an}(\zeta) = \frac{\phi_0 g^*(p)(s_a+\zeta)S_-(-s_h)\tilde{c}_{44}}{\sqrt{s_\ell-\zeta}(s_{bg}+\zeta)\mathcal{T}_+(\zeta)D_s}, \tag{75}$$

where $R_-(\zeta)$ and $\mathcal{T}_+(\zeta)$ are sectionally analytic functions given in the Appendix.

To this end, from Eqs. (72)–(75), the coefficients of $A^l(\zeta)$, $B^l(\zeta)$, $A^u(\zeta)$, and $B^u(\zeta)$ can be found:

$$A^l(\zeta) = A_{sy}(\zeta) + A_{an}(\zeta) = -\left(\sigma_0 + \frac{e_{15}\sqrt{s_\ell+\zeta}\sqrt{s_a+s_h}\sqrt{s_\ell+s_h}}{\sqrt{s_a-\zeta}}\phi_0\right)K(\zeta), \tag{76}$$

$$B^l(\zeta) = B_{sy}(\zeta) + B_{an}(\zeta) = \left(\frac{e_{15}}{\epsilon_{11}}C_f\sigma_0 + \frac{\tilde{c}_{44}\sqrt{s_a+\zeta}\sqrt{s_a+s_h}\sqrt{s_\ell+s_h}}{\sqrt{s_\ell-\zeta}}\phi_0\right)K(\zeta), \tag{77}$$

$$A^u(\zeta) = A_{sy}(\zeta) - A_{an}(\zeta) = -\left(\sigma_0 - \frac{e_{15}\sqrt{s_\ell+\zeta}\sqrt{s_a+s_h}\sqrt{s_\ell+s_h}}{\sqrt{s_a-\zeta}}\phi_0\right)K(\zeta), \tag{78}$$

$$B^u(\zeta) = B_{sy}(\zeta) - B_{an}(\zeta) = \left(\frac{e_{15}}{\epsilon_{11}}C_f\sigma_0 - \frac{\tilde{c}_{44}\sqrt{s_a+\zeta}\sqrt{s_a+s_h}\sqrt{s_\ell-s_h}}{\sqrt{s_\ell-\zeta}}\phi_0\right)K(\zeta), \tag{79}$$

where

$$K(\zeta) \coloneqq \left(\frac{g^*(p)(s_{bg}-\zeta)\sqrt{s_a+s_h}\mathcal{T}_-(\zeta)}{(\zeta+s_h)\sqrt{s_a-\zeta}(s_{bg}+s_h)\mathcal{T}_-(-s_h)BG(\zeta)}\right). \tag{80}$$

Substituting Eqs. (76)–(79) into Eqs. (32) and (33) and performing an inverse transform, one obtains the scattered displacement and pseudo-electric wave fields:

$$w^*(x,y,p) = -\frac{1}{2\pi ip}\int_{\zeta_\alpha-i\infty}^{\zeta_\alpha+i\infty}\left\{\left(\sigma_0 + \mathrm{sgn}(y)\frac{e_{15}\sqrt{s_\ell+\zeta}\sqrt{s_a+s_h}\sqrt{s_\ell+s_h}}{\sqrt{s_a-\zeta}}\phi_0\right)\cdot K(\zeta)\right\} \times\exp[-p(\alpha(\zeta)\mathrm{sgn}(y)y - \zeta x)]d\zeta, \tag{81}$$

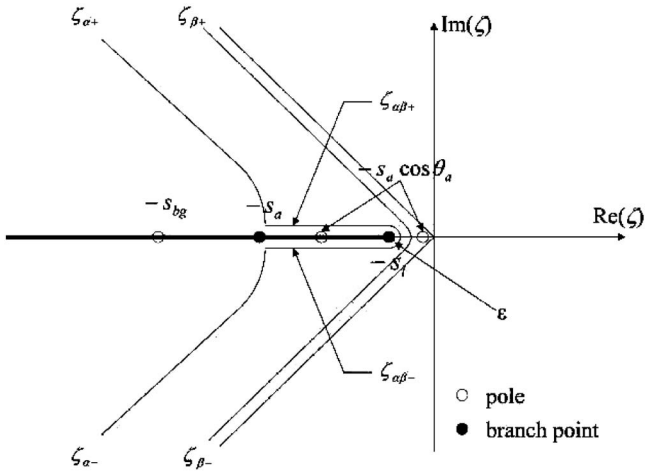

Fig. 2 The Cagniard-deHoop inversion paths Γ_α, Γ_β, and $\Gamma_{\alpha\beta}$ for acoustic excitation

$$\psi^*(x,y,p)=\frac{1}{2\pi ip}\int_{\zeta_{\beta^-}-i\infty}^{\zeta_{\beta^+}+i\infty}\left[\left(\frac{e_{15}}{\epsilon_{11}}C_f\sigma_0+\mathrm{sgn}(y)\frac{\tilde{c}_{44}\sqrt{s_a+\zeta}\sqrt{s_a+s_h}\sqrt{s_\ell+s_h}}{\sqrt{s_\ell-\zeta}}\phi_0\right)\cdot K(\zeta)\right]\times\exp[-p(\beta(\zeta)\mathrm{sgn}(y)y-\zeta x)]d\zeta. \quad (82)$$

4 Scattering Fields

4.1 Cagniard-deHoop Inversion. Having carried out the Wiener-Hopf decomposition, we are now in a position to invert the integrals in Eqs. (81) and (82) to obtain explicit solutions in the physical domain. The exact inversion can be achieved by the Cagniard-de Hoop scheme [32,33]. First, the scattered displacement and the pseudo-electric potential fields for an incident acoustic wave are considered so that $s_h=s_a\cos(\theta_a)$ in the integrals. We proceed by replacing the original Bromwich path by a deformed Cagniard contour such that the one-sided Laplace transform can be obtained by inspection. In the following, the inversion procedure is presented only for $y>0$; the inversion procedure for $y<0$ is identical and is omitted.

Shown in Fig. 2, the following inversion paths are chosen: Γ_α, $\Gamma_{\alpha\beta}$, and Γ_β, in which

$$\alpha(\zeta)y-\zeta x=t,\quad \zeta\in\Gamma_\alpha,\Gamma_{\alpha\beta}$$
$$\beta(\zeta)y-\zeta x=t,\quad \zeta\in\Gamma_\beta. \quad (83)$$

Let $x=r\cos\theta$ and $y=r\sin\theta$. One then has

$$\zeta_{\alpha\pm}=\frac{1}{r}\left(-t\cos\theta\pm i\sin\theta\sqrt{t^2-s_a^2r^2}\right),\quad s_ar\leqslant t<\infty \quad (84)$$

$$\zeta_{\alpha\beta\pm}=\frac{1}{r}\left(-t\cos\theta\pm\sin\theta\sqrt{s_a^2r^2-t^2}\right)\pm i\epsilon,\quad t_{\alpha0}\leqslant t<s_ar \quad (85)$$

$$\zeta_{\beta\pm}=\frac{1}{r}\left(-t\cos\theta\pm i\sin\theta\sqrt{t^2-s_\ell^2r^2}\right),\quad s_\ell r\leqslant t\leqslant\infty \quad (86)$$

where $t_{\alpha0}=\sqrt{s_a^2-s_\ell^2}y+s_\ell x$.

It should be noted that at $\zeta=-s_a\cos\theta$, the path Γ_α intercepts the real axis Re(ζ). Thus, a supplement path $\Gamma_{\alpha\beta}$ is needed to circumvent the branch cut of multivalued function $\beta(\zeta)=\sqrt{s_\ell^2-\zeta^2}$. This leads to the occurrence of the electroacoustic head wave (see discussions in [13] as well as [15]). Along path $\Gamma_{\alpha\beta}$, the parameter θ varies in the range

$$0\geqslant\theta\geqslant\theta_{cr}^{a\ell} \quad (87)$$

where $\theta_{cr}^{a\ell}:=|\cos^{-1}(s_\ell/s_a)|$.

Following de Hoop [33], one may show that

$$\frac{\partial\zeta_{\alpha\pm}}{\partial t}=\frac{\pm i\alpha(\zeta_{\alpha\pm})}{\sqrt{t^2-s_a^2r^2}};\quad \alpha(\zeta_{\alpha\pm})=\frac{\sin\theta}{r}t\pm i\frac{\cos\theta}{r}\sqrt{t^2-s_a^2r^2}; \quad (88)$$

$$\frac{\partial\zeta_{\alpha\beta\pm}}{\partial t}=\frac{\mp\alpha(\zeta_{\alpha\beta\pm})}{\sqrt{s_a^2r^2-t^2}};\quad \alpha(\zeta_{\alpha\beta\pm})=\frac{\sin\theta}{r}t\pm\frac{\cos\theta}{r}\sqrt{s_a^2r^2-t^2}; \quad (89)$$

$$\frac{\partial\zeta_{\beta\pm}}{\partial t}=\frac{\pm i\beta(\zeta_{\beta\pm})}{\sqrt{t^2-s_\ell^2r^2}};\quad \beta(\zeta_{\beta\pm})=\frac{\sin\theta}{r}t\pm i\frac{\cos\theta}{r}\sqrt{t^2-s_\ell^2r^2}; \quad (90)$$

and subsequently exact inversions are found:

$$w^{(s)}(x,y,t)=\int_0^t G(t-\tau)w_\delta^{(s)}(x,y,\tau)d\tau+w_r^{(s)}(x,y,t)$$
$$\psi^{(s)}(x,y,t)=\int_0^t G(t-\tau)\psi_\delta^{(s)}(x,y,\tau)d\tau+\psi_r^{(s)}(x,y,t) \quad (91)$$

where the subscript "δ" represents the scattering fields due to the impulsive incident wave, and $w_r^{(s)}$, $\psi_r^{(s)}$ are reflected/refracted displacement and pseudo-electric fields.

$$w_\delta^{(s)}(x,y,t)=-\frac{1}{\pi}\left\{\Re\left[\left(\sigma_0+\mathrm{sgn}(y)\frac{e_{15}\sqrt{s_\ell+\zeta_{\alpha+}}\sqrt{s_a+s_h}\sqrt{s_\ell+s_h}}{\sqrt{s_a-\zeta_{\alpha+}}}\phi_0\right)\cdot\left(\frac{(s_{bg}-\zeta_{\alpha+})\sqrt{s_a+s_h}\mathcal{T}_-(\zeta_{\alpha+})}{(\zeta_{\alpha+}+s_h)\sqrt{s_a-\zeta_{\alpha+}}(s_{bg}+s_h)\mathcal{T}_-(-s_h)BG(\zeta_{\alpha+})}\right)\frac{\alpha(\zeta_{\alpha+})}{\sqrt{t^2-s_a^2r^2}}\right]\cdot H(t-s_ar)-\Im\left[\left(\sigma_0+\mathrm{sgn}(y)\frac{e_{15}\sqrt{s_\ell+\zeta_{\alpha\beta+}}\sqrt{s_a+s_h}\sqrt{s_\ell+s_h}}{\sqrt{s_a-\zeta_{\alpha\beta+}}}\phi_0\right)\cdot\left(\frac{(s_{bg}-\zeta_{\alpha\beta+})\sqrt{s_a+s_h}\mathcal{T}_-(\zeta_{\alpha\beta+})}{(\zeta_{\alpha\beta+}+s_h)\sqrt{s_a-\zeta_{\alpha\beta+}}(s_{bg}+s_h)\mathcal{T}_-(-s_h)BG(\zeta_{\alpha\beta+})}\right)\times\frac{\alpha(\zeta_{\alpha\beta+})}{\sqrt{t^2-s_a^2r^2}}\right]\cdot[H(t-t_{\alpha0})-H(t-s_ar)]\right\}, \quad (92)$$

$$\psi_\delta^{(s)}(x,y,t)=\frac{1}{\pi}\left[\left(\frac{e_{15}}{\epsilon_{11}}C_f\sigma_0+\mathrm{sgn}(y)\frac{\tilde{c}_{44}\sqrt{s_a+\zeta_{\beta+}}\sqrt{s_a+s_h}\sqrt{s_\ell+s_h}}{\sqrt{s_\ell-\zeta_{\beta+}}}\phi_0\right)\left(\frac{(s_{bg}-\zeta_{\beta+})\sqrt{s_a+s_h}\mathcal{T}_-(\zeta_{\beta+})}{(\zeta_{\beta+}+s_h)\sqrt{s_a-\zeta_{\beta+}}(s_{bg}+s_h)\mathcal{T}_-(-s_h)BG(\zeta_{\beta+})}\right)\frac{\beta(\zeta_{\beta+})}{\sqrt{t^2-s_\ell^2r^2}}\right]\cdot H(t-s_\ell r). \quad (93)$$

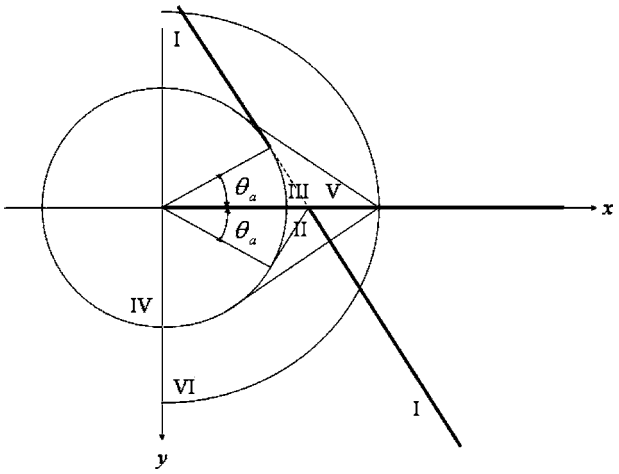

Fig. 3 The scattering patterns excited by an acoustic source: case (1)

4.2 Scattering Fields in Front of the Crack Tip. Scattering fields due to different incident waves in front of the crack tip are discussed as follows:

4.2.1 Incident Acoustic Plane Wave. In diffraction theory, both the acoustic and the electromagnetic, the simple pole that represents the incident source determines the geometrical reflection/refraction patterns. These geometrical scattering patterns induced by acoustic excitation depend on the incident angle of the acoustic wave, because the position of simple pole relies on the angle of incident acoustic wave. Figure 2 shows that there are two different positions of the simple pole, $\zeta=-s_h=-s_a\cos(\theta_a)$, and the positions of $-s_h$ in the ζ plane will directly affect the outcome of the reflection and refraction fields. There are basically two cases:

(1) $s_a\cos(\theta_a)>s_\ell$

In this case, the pole always lies to the right of Γ_α but to the left of Γ_β and $\Gamma_{\beta'}$. This means that there are pole contributions to the paths Γ_α, but no contributions to the paths Γ_β. After evaluating the residues of the poles for the corresponding integral in (81) and (82), we have

$$w_r^{(s)}(x,y,t)=\begin{cases}\Re\left(\dfrac{s_a\sin(\theta_a)+\tilde{k}_e^2\sqrt{s_\ell^2-[s_a\cos(\theta_a)]^2}}{s_a\sin(\theta_a)-\tilde{k}_e^2\sqrt{s_\ell^2-[s_a\cos(\theta_a)]^2}}\right)\cdot w_o^{(i)}G(t-s_a[\cos(\theta_a)x+\sin(\theta_a)y]) & \\ -\Im\left(\dfrac{s_a\sin(\theta_a)+\tilde{k}_e^2\sqrt{s_\ell^2-[s_a\cos(\theta_a)]^2}}{s_a\sin(\theta_a)-\tilde{k}_e^2\sqrt{s_\ell^2-[s_a\cos(\theta_a)]^2}}\right)\cdot w_o^{(i)}\mathcal{H}\{G(t-s_a[\cos(\theta_a)x+\sin(\theta_a)y])\}, & 0\leqslant\theta<\theta_a;\\ 0, & \theta_a\leqslant\theta<\pi;\\ 0, & \pi\leqslant\theta<2\pi-\theta_a;\\ -w_o^{(i)}G(t-s_a[\cos(\theta_a)x-\sin(\theta_a)y]), & 2\pi-\theta_a\leqslant\theta<2\pi,\end{cases}\tag{94}$$

$$\psi_r^{(s)}(x,y,t)=\begin{cases}0, & 0\leqslant\theta<\pi;\\ 0, & \pi\leqslant\theta<2\pi;\end{cases}\tag{95}$$

where the Hilbert transform $\mathcal{H}\{\cdot\}$ is defined as

$$\mathcal{H}\{f(t)\}=\frac{1}{\pi}PV\int_{-\infty}^{\infty}\frac{f(\tau)}{\tau-t}d\tau,\tag{96}$$

where *PV* denotes the Cauchy principal value.

The complete scattering pattern is shown in Fig. 3. Note that the refracted acoustic wave (dashed line in the figure) completely cancels the incident acoustic wave.

(2) $s_\ell\geqslant s_a\cos(\theta_a)$

In this case, the pole lies to the right of all the paths, and, therefore, after evaluating the residues of the poles for all the corresponding integrals, we have

$$w_r^{(s)}(x,y,t)=\begin{cases}\left(\dfrac{s_a\sin(\theta_a)+\tilde{k}_e^2 s_\ell\sin(\theta_\ell)}{s_a\sin(\theta_a)-\tilde{k}_e^2 s_\ell\sin(\theta_\ell)}\right)\cdot w_o^{(i)}G(t-s_a[\cos(\theta_a)x+\sin(\theta_a)y]), & 0\leqslant\theta<\theta_a;\\ 0, & \theta_a\leqslant\theta<\pi;\\ 0, & \pi\leqslant\theta<2\pi-\theta_a;\\ -w_o^{(i)}G(t-s_a[\cos(\theta_a)x-\sin(\theta_a)y]), & 2\pi-\theta_a\leqslant\theta<2\pi,\end{cases}\tag{97}$$

$$\psi_r^{(s)}(x,y,t)=\begin{cases}\left(\dfrac{-2e_{15}C_f s_a\sin(\theta_a)}{\epsilon_{11}(s_a\sin(\theta_a)-\tilde{k}_e^2 s_\ell\sin(\theta_\ell))}\right)\cdot w_o^{(i)}G(t-[s_a\cos(\theta_a)x+s_\ell\sin(\theta_\ell)y]), & 0\le\theta<\theta_\ell;\\ 0, & \theta_\ell\le\theta<\pi;\\ 0, & \pi\le\theta<2\pi-\theta_\ell;\\ 0, & 2\pi-\theta_\ell\le\theta<2\pi.\end{cases} \tag{98}$$

The complete scattering pattern is shown in Fig. 4. Again, the refracted acoustic wave (dashed line in the figure) completely cancels the incident acoustic wave.

In both cases, one can observe that a refracted acoustic wave is passing through the slit, which will not happen in purely elastic media.

4.2.2 Incident Electric Plane Wave. As shown in Fig. 5, the simple pole $\zeta=-s_h=-s_\ell\cos(\theta_\ell)$ always lies to the right of all the integration paths, and thus the residue of the pole due to the corresponding integral needs to be evaluated. Therefore, the reflection and refraction fields due to an incident pseudo-electric source are

$$w_r^{(s)}(x,y,t)=\begin{cases}\left(\dfrac{2e_{15}s_\ell\sin(\theta_\ell)}{\tilde{c}_{44}(s_a\sin(\theta_a)-\tilde{k}_e^2 s_\ell\sin(\theta_\ell))}\right)\cdot\psi_o^{(i)}G(t-[s_\ell\cos(\theta_\ell)x+s_a\sin(\theta_a)y]), & 0\le\theta<\theta_a;\\ 0, & \theta_a\le\theta<\pi;\\ 0, & \pi\le\theta<2\pi-\theta_a;\\ 0, & 2\pi-\theta_a\le\theta<2\pi,\end{cases} \tag{99}$$

$$\psi_r^{(s)}(x,y,t)=\begin{cases}-\left(\dfrac{s_a\sin(\theta_a)+\tilde{k}_e^2 s_\ell\sin(\theta_\ell)}{s_a\sin(\theta_a)-\tilde{k}_e^2 s_\ell\sin(\theta_\ell)}\right)\cdot\psi_o^{(i)}G(t-s_\ell[\cos(\theta_\ell)x+\sin(\theta_\ell)y]), & 0\le\theta<\theta_\ell;\\ 0, & \theta_\ell\le\theta<\pi;\\ 0, & \pi\le\theta<2\pi-\theta_\ell;\\ -\psi_o^{(i)}G(t-s_\ell[\cos(\theta_\ell)x-\sin(\theta_\ell)y]), & 2\pi-\theta_\ell\le\theta<2\pi.\end{cases} \tag{100}$$

The complete scattering pattern is shown in Fig. 6. Note that the refracted electric wave (dashed line in the figure) completely cancels the incident electric wave.

5 Discussions

5.1 Displacement Time History. With the analytical expressions of the diffracted waves, the displacement time history at a fixed point can be traced and calculated during the electroacoustic scattering so that we may be able to compare them with the measurements obtained in the nondestructive testing. Figures 7 and 8 show the displacement time histories at various θ with fixed y in the upper half space due to an impulsive incident acoustic source and an electric source, respectively, with Fig. 7 corresponding to acoustic source case (1) in the previous section. Recall that θ is measured clockwise beginning from the x axis, so that with y fixed, $\theta=-90$ deg in both figures is closest to the crack tip while $\theta=-10$ deg is the farthest. A distinctive feature of scattering by a conducting crack is the ability of the head wave to tunnel through the crack, a phenomenon which is not observed in the purely elastic case in [34]. Note that in Figs. 7 and 8 the head wave arrives at almost identical times at each θ in both figures. Since the speed of light is much larger than the acoustic wave speed, the head wave wavefront is almost parallel to the crack. (Imagine the

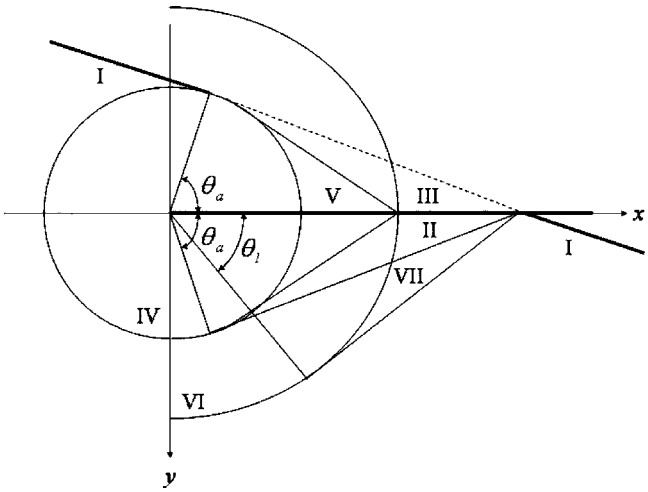

Fig. 4 The scattering patterns excited by an acoustic source: case (2)

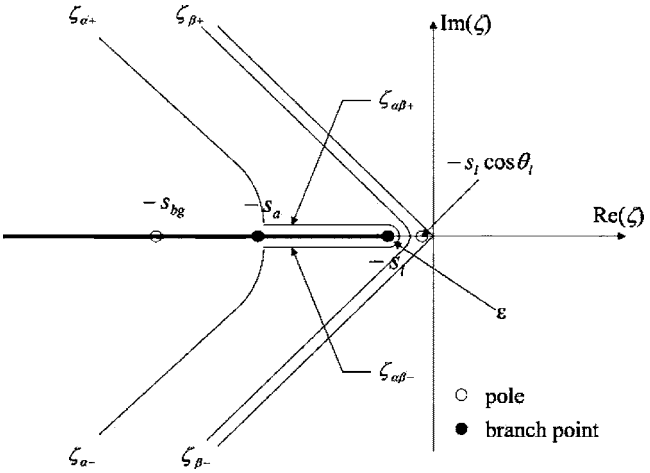

Fig. 5 The Cagniard-deHoop inversion paths for pseudo-electric excitation

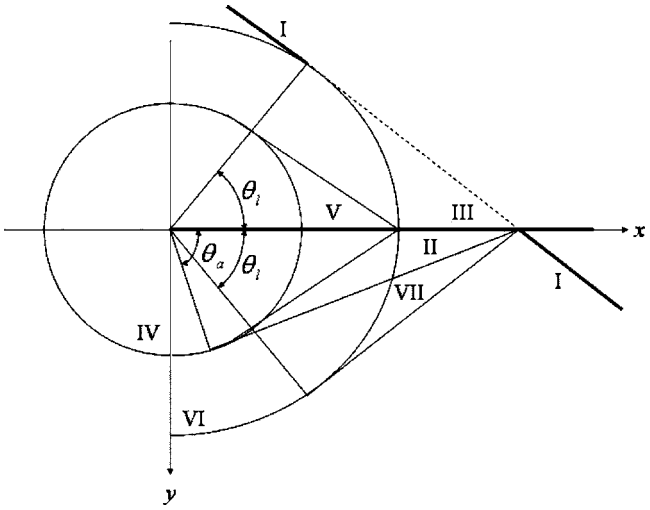

Fig. 6 The scattering patterns excited by an electric source

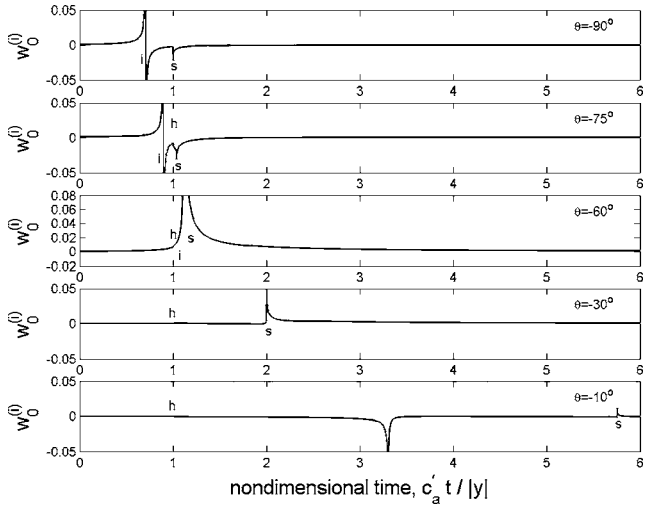

Fig. 7 Displacement-time histories at various θ with fixed y due to an impulsive acoustic source incident at θ_a=45°. Labels: i=incident wave, h=head wave, and s=scattered wave.

arc next to "**V**" in Figs. 3–6 is much larger. Then the electroacoustic head wave line connecting the arc would be more parallel to the crack.). This electromagnetic acoustic head wave has also been observed in experiments, e.g., [35]. Another distinctive feature of the scattering field is the cancellation of the refracted acoustic wave by the incident acoustic wave as seen in equations (95) and (98) and, thus, no diffracted acoustic wave or incident acoustic wave exists in the displacement time histories for $|\theta| < |\theta_a|$. Also, the scattered acoustic wave originating from the crack tip can be observed in both time histories as decreasing in magnitude as the observation point is moving farther away from the crack tip.

5.2 Mode Conversion and Reflection/Refraction Coefficients. As shown above, in a piezoelectric medium an acoustic incident wave can trigger both acoustic and electric scattering fields, and vice versa an electric incident wave can generate both acoustic and electric scattering fields as well. It would be interesting to examine the possible mode conversion between these geometrical reflection/refraction waves. To do so, similar convention used by Aki and Richards [36] for purely elastic wave reflection conversion is adopted here. The ratios of all possible mode conversions are defined and calculated as follows,

$$\acute{A}\acute{A} := \frac{w_r^{(s)}}{w^{(i)}} = -1, \quad \pi \leqslant \theta < 2\pi \tag{101}$$

$$\acute{A}\acute{E} := \frac{\psi_r^{(s)}}{w^{(i)}} = 0, \quad \pi \leqslant \theta < 2\pi \tag{102}$$

$$\acute{E}\acute{A} := \frac{w_r^{(s)}}{\psi^{(i)}} = 0, \quad \pi \leqslant \theta < 2\pi \tag{103}$$

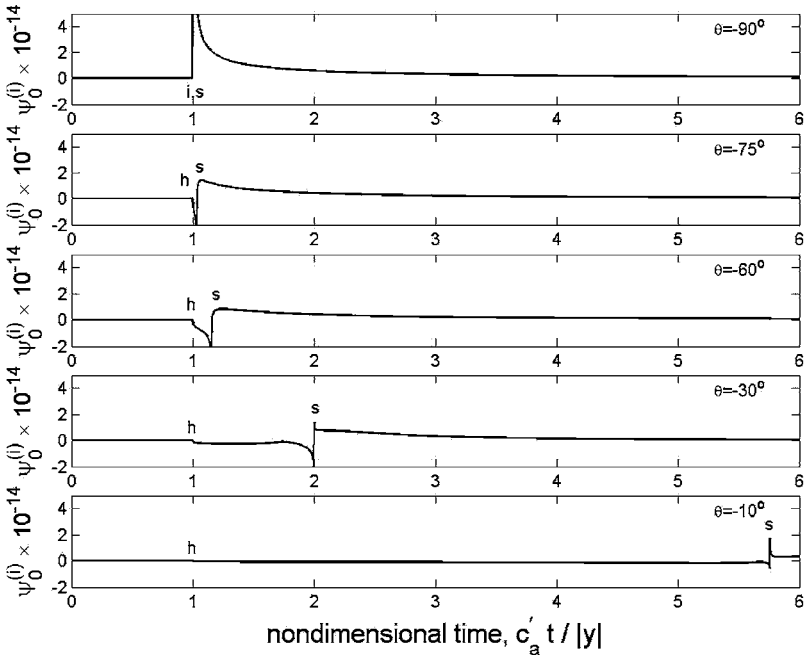

Fig. 8 Displacement time histories at various θ with fixed y due to an impulsive electric source incident at θ_ℓ=45°. Labels: i=incident wave, h=head wave, and s=scattered wave.

$$\acute{E}\acute{E} := \frac{\psi_r^{(s)}}{\psi^{(i)}} = -1, \quad \pi \leqslant \theta < 2\pi \tag{104}$$

$$\acute{A}\grave{A} := \frac{\omega_r^{(s)}}{w^{(i)}} = \frac{s_a \sin(\theta_a) + \tilde{k}_e^2 s_\ell \sin(\theta_\ell)}{s_a \sin(\theta_a) - \tilde{k}_e^2 s_\ell \sin(\theta_\ell)}, \quad 0 \leqslant \theta < \pi \tag{105}$$

$$\acute{A}\grave{E} := \frac{\psi_r^{(s)}}{w^{(i)}} = \frac{-2e_{15}C_f s_a \sin(\theta_a)}{\epsilon_{11}(s_a \sin(\theta_a) - \tilde{k}_e^2 s_\ell \sin(\theta_\ell))}, \quad 0 \leqslant \theta < \pi \tag{106}$$

$$\acute{E}\grave{A} := \frac{w_r^{(s)}}{\psi^{(i)}} = \frac{2e_{15}s_\ell \sin(\theta_\ell)}{\tilde{c}_{44}(s_a \sin(\theta_a) - \tilde{k}_e^2 s_\ell \sin(\theta_\ell))}, \quad 0 \leqslant \theta < \pi \tag{107}$$

$$\acute{E}\grave{E} := \frac{\psi_r^{(s)}}{\psi^{(i)}} = -\frac{s_a \sin(\theta_a) + \tilde{k}_e^2 s_\ell \sin(\theta_\ell)}{s_a \sin(\theta_a) - \tilde{k}_e^2 s_\ell \sin(\theta_\ell)}, \quad 0 \leqslant \theta < \pi \tag{108}$$

5.3 Dynamic Intensity Factors. At the tip of the screen or the crack, scattering fields will become singular, which is of great importance for material strength. In what follows, the intensity factors of the singular fields generated by the antisymmetry solutions are calculated. Define

$$K_\sigma(t) := \lim_{x\to 0^-} \sqrt{2\pi|x|}\,\sigma_{yz}^{(s)}(x,0,t), \tag{109}$$

$$K_D(t) := \lim_{x\to 0^-} \sqrt{2\pi|x|}\,D_y^{(s)}(x,0,t), \tag{110}$$

$$K_E(t) := \lim_{x\to 0^-} \sqrt{2\pi|x|}\,E_y^{(s)}(x,0,t). \tag{111}$$

Considering the asymptotic relations [37],

$$\lim_{x\to 0^-} (\pi|x|)^{1/2}\sigma_{yz}^*(x,0,p) = \lim_{\zeta\to-\infty} |p\zeta|^{1/2}\frac{\Sigma_-(\zeta,p)}{p} \tag{112}$$

$$\lim_{x\to 0^-} (\pi|x|)^{1/2}D_y^*(x,0,p) = \lim_{\zeta\to-\infty} |p\zeta|^{1/2}\hat{D}_y^*(\zeta,p) \tag{113}$$

$$\lim_{x\to 0^-} (\pi|x|)^{1/2}E_y^*(x,0,p) = \lim_{\zeta\to-\infty} |p\zeta|^{1/2}\hat{E}_y^*(\zeta,p), \tag{114}$$

one can derive that

$$K_\sigma^*(p) = \sqrt{2}\frac{\sigma_0\sqrt{s_a+s_h}}{\mathcal{T}_-(-s_h)(s_{bg}+s_h)}\left(\frac{-g^*(p)}{\sqrt{p}}\right) \tag{115}$$

After performing inverse Laplace transform, one may obtain

$$K_\sigma(t) = -\frac{\sigma_0\sqrt{s_a+s_h}}{\mathcal{T}_-(-s_h)(s_{bg}+s_h)}\chi(t) \tag{116}$$

where

$$\chi(t) := \sqrt{\frac{2}{\pi}}\int_{+0}^{t}\frac{1}{\sqrt{\tau}}g(t-\tau)d\tau \tag{117}$$

Similarly, based on the definition

$$\hat{D}_y^*(\zeta,p) = [-e_{15}(1-C_f)\alpha(\zeta)A(\zeta) + \epsilon_{11}\beta(\zeta)B(\zeta)]/p, \tag{118}$$

$$\hat{E}_y^*(\zeta,p) = \left(\alpha(\zeta)A(\zeta) + \frac{e_{15}}{\epsilon_{11}}C_f\beta(\zeta)B(\zeta)\right)/p, \tag{119}$$

one can then show that

$$K_D(t) = -[e_{15}\sigma_0\chi(t) + (e_{15}^2(1-C_f) + \tilde{c}_{44}\epsilon_{11})\sqrt{s_a+s_h}\sqrt{s_\ell+s_h}\phi_0\mathcal{H}\{\chi(t)\}] \cdot \frac{\sqrt{s_a+s_h}}{\tilde{c}_{44}(1-\tilde{k}_e^2)\mathcal{T}_-(-s_h)(s_{bg}+s_h)}, \tag{120}$$

$$K_E(t) = -\left[\left(1+\frac{e_{15}^2}{\epsilon_{11}^2}C_f^2\right)\sigma_0\chi(t) + \left(e_{15}+\frac{e_{15}}{\epsilon_{11}}C_f\tilde{c}_{44}\right)\times\sqrt{s_a+s_h}\sqrt{s_\ell+s_h}\phi_0\mathcal{H}\{\chi(t)\}\right] \cdot \frac{\sqrt{s_a+s_h}}{\tilde{c}_{44}(1-\tilde{k}_c^2)\mathcal{T}_-(-s_h)(s_{bg}+s_h)}. \tag{121}$$

Define the following stress, electric displacement, and electric field phase functions in the Laplace transform domain as

$$G_\sigma(s_h) := \frac{K_\sigma^*(p)}{\chi^*(p)} = -\frac{\sigma_0\sqrt{s_a+s_h}}{\mathcal{T}_-(-s_h)(s_{bg}+s_h)} \tag{122}$$

$$G_D(s_h) := \frac{K_D^*(p)}{\chi^*(p)} = -\{e_{15}\sigma_0 + i\,\mathrm{sgn}(p)[e_{15}^2(1-C_f) + \tilde{c}_{44}\epsilon_{11}] \cdot \sqrt{s_a+s_h}\sqrt{s_\ell+s_h}\phi_0\}\frac{\sqrt{s_a+s_h}}{\tilde{c}_{44}(1-\tilde{k}_e^2)\mathcal{T}_-(-s_h)(s_{bg}+s_h)} \tag{123}$$

$$G_E(s_h) := \frac{K_E^*(p)}{\chi^*(p)} = -\left[\left(1+\frac{e_{15}^2}{\epsilon_{11}^2}C_f^2\right)\sigma_0 + i\,\mathrm{sgn}(p)\left(e_{15}+\frac{e_{15}}{\epsilon_{11}}C_f\tilde{c}_{44}\right) \cdot \sqrt{s_a+s_h}\sqrt{s_\ell+s_h}\phi_0\right]\frac{\sqrt{s_a+s_h}}{\tilde{c}_{44}(1-\tilde{k}_e^2)\mathcal{T}_-(-s_h)(s_{bg}+s_h)} \tag{124}$$

Apparently, the electric displacement and electric field are functions of the frequency of the incident shape function.

Figures 9–11 display the phase functions G_σ, G_D, and G_E, which are normalized by the incident acoustic wave amplitude w_0 or the incident electric wave amplitude ψ_0 at its respective incident angle for a broad range of electromechanical coupling coefficients ($\tilde{k}_e$). In general, the amplitude of the normalized phase function increases with increasing electromechanical coupling coefficient. Examining the normalized stress phase functions G_σ in Figs. 9(*a*) and 9(*b*), the amplitude increases with the increase of incident angle, because more work is done on the crack tip by incident waves at large angles. Also, the amplitude of the normalized stress phase function due to an incident acoustic source is much larger than that due to an electric source. The amplitude of the electric displacement and electric field phase functions G_D and G_E due to an incident acoustic wave and an incident electric wave are plotted in Figs. 10 and 11, respectively. In general, the amplitudes of both functions decrease with the increase of incident angles. There are two competing effects here: as incident angle increases, the incident wave is more focused on opening the crack; on the other hand, when the horizontal slowness of the wave decreases, the wave has less time to do work on the crack. The former effect is much more significant in mechanical stress analysis, but the latter effect is more pronounced for the electric displacement and electric field. The most striking fact is that the amplitudes for both phase functions are significantly larger for an incident acoustic source than for that of an electric source, and thus the large electromechanical coupling plays an important role in the increase of electric displacement and electric field intensities.

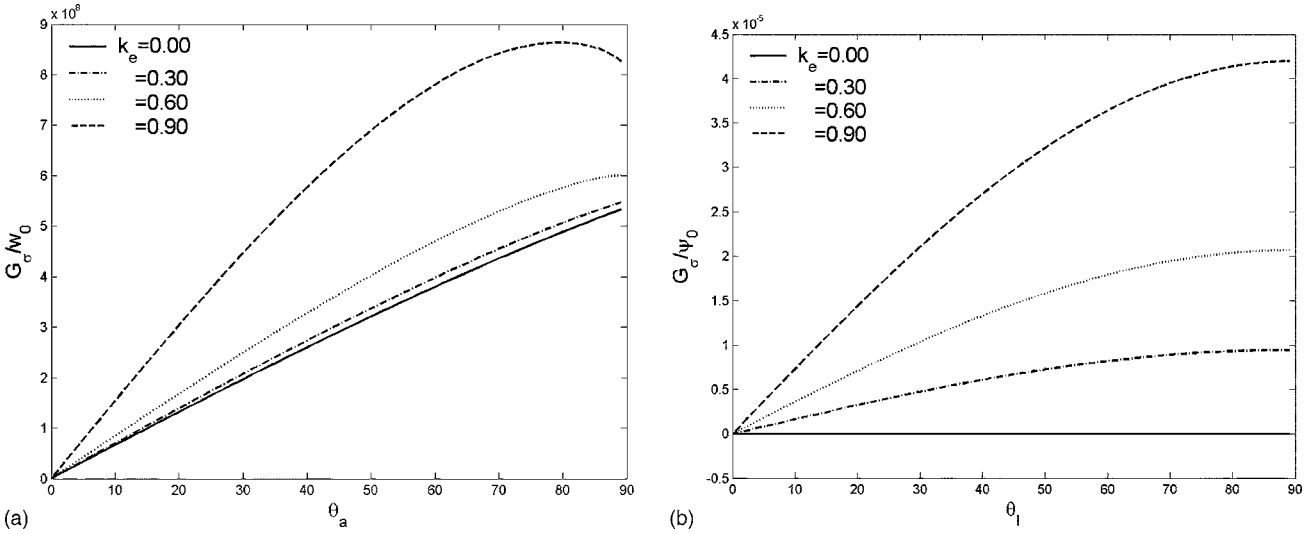

Fig. 9 Amplitude of the normalized stress phase function for various electro-mechanical coupling coefficients ($\tilde{k}_e$) (*a*) versus incident angle for an incident acoustic source G_σ/w_0 and (*b*) versus incident angle for an incident electric source G_σ/ψ_0

6 Conclusions

In this work, a complete solution of a Kirchhoff diffraction problem in a piezoelectric medium is obtained. It is not possible to obtain such solution by employing the quasi-static approximation that has been used traditionally in the design of ferroelectric sensors. Under the quasi-static approximation, the initial boundary value problem becomes ill-posed, because the corresponding wave equations are not hyperbolic anymore.

As shown in [15], the characteristics of the scattering patterns in piezoelectric media have major differences from that in elastic media. For instance, considering the scattering field generated by an SH acoustic incident wave, there is no "shadow zone" behind the half-plane slit in a piezoelectric media, which is in contrast with the similar case in a purely elastic media [38]. In other words, the crack is somewhat "transparent" to incident waves. This is because in a piezoelectric medium the incident acoustic/electric wave interacts with the crack to produce the electro-acoustic head wave that can penetrate the crack surface as shown in Figs. 3, 4, and 6.

Another interesting feature of the scattering fields is that the different head waves exist in many different scenarios, which is a much richer physical phenomenon than the scattering field in a purely elastic medium.

Moreover, it may be observed that the critical angle $\theta_{cr}^{a\ell}$ dictates the reflection pattern. For example, when the incident acoustic angle is smaller than the critical angle, there will be no reflected electric wave as shown in Fig. 3.

To the best of the authors' knowledge, up to this date, there is no systematic experimental study on the Kirchhoff diffraction in piezoelectric/ferroelectric materials. We have not found any experimental data of the Kirchhoff diffraction in piezoelectric materials in open literature. Nevertheless, some of the scattered wave modes and head wave modes predicted in this paper are in good agreement with the experimental data obtained from an experiment of the transient surface excitation of a piezoelectric material (see [35,39]), which cannot be predicted by the commonly used quasi-static approximation theory at all.

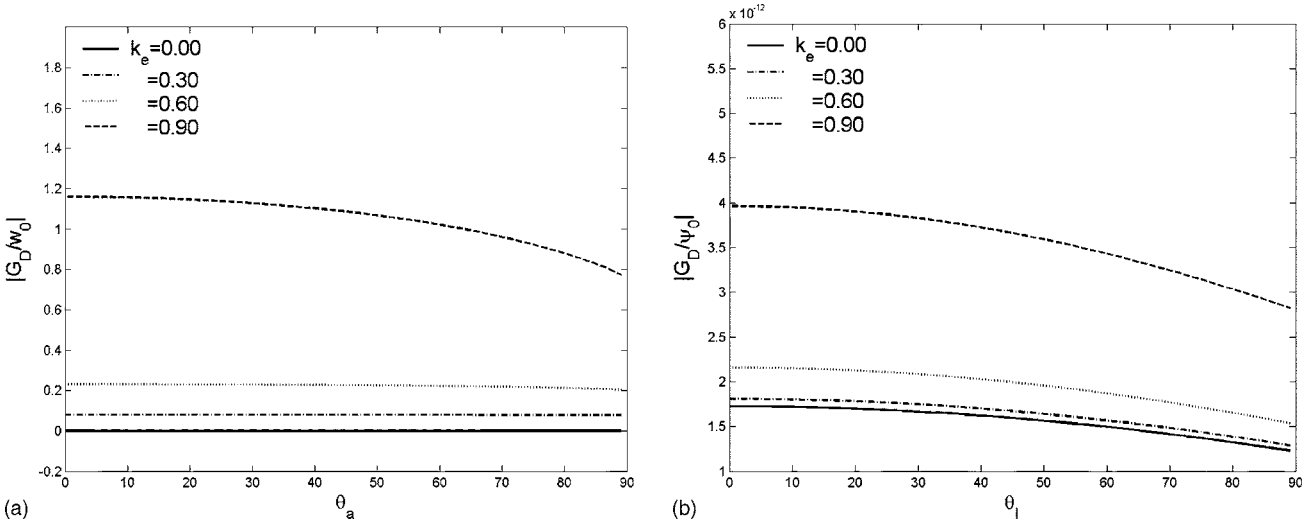

Fig. 10 Amplitude of the normalized electric displacement phase function for various electro-mechanical coupling coefficients ($\tilde{k}_e$) (a) versus an incident acoustic source G_D/w_0 and (b) versus an incident electric source G_D/ψ_0

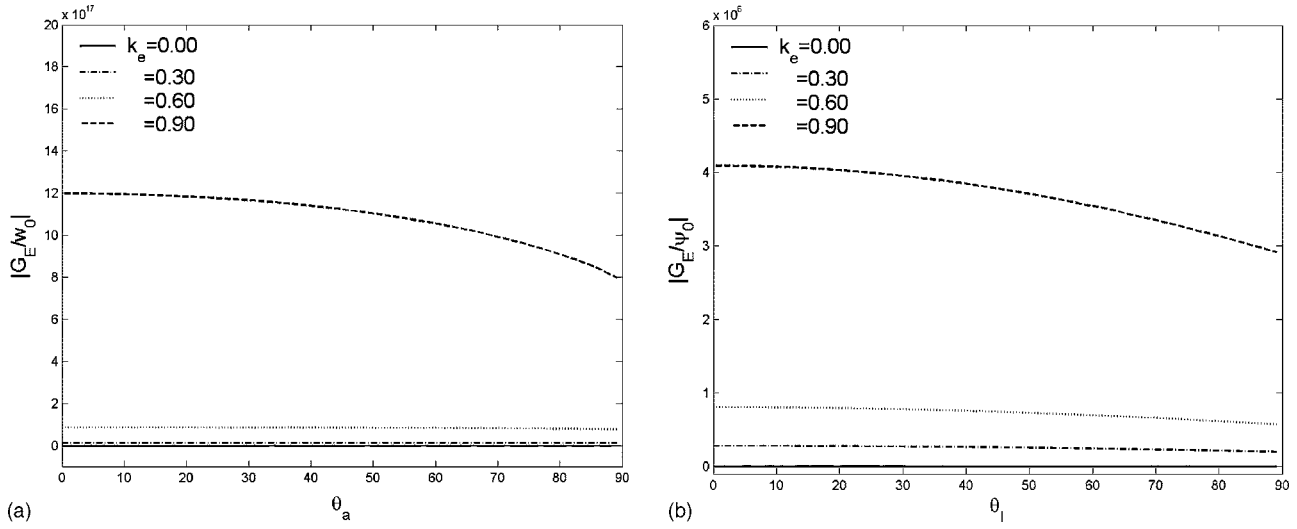

Fig. 11 Amplitude of the normalized electric field phase function for various electro-mechanical coupling coefficients ($\tilde{k}_e$) (a) versus an incident acoustic source G_E/w_0 and (b) versus an incident electric source G_E/ψ_0

Acknowledgments

This research is supported by a grant from NSF (Grant No. CMS-0239130) (SL), and by Jane Lewis Fellowship from University of California, Berkeley (ACT), and another grant from NSF (Grant No. CMS-9908218) (SDG), which are gratefully acknowledged.

Appendix: Solution of the Wiener-Hopf Equations

The key to solving the two Wiener-Hopf equations (58) and (59) is how to factorize the Bleustein-Gulyaev function $BG(\zeta)$ into sectionally analytic functions in the left and right half complex-ζ planes, respectively. This has been done by Li and Mataga [40] and by Li [13],

$$BG(\zeta)=\frac{(s_{bg}+\zeta)(s_{bg}-\zeta)}{\sqrt{s_a+\zeta}(s_a-\zeta)}\mathcal{T}_+(\zeta)\mathcal{T}_-(\zeta)D_s \tag{A1}$$

where

$$D_s := \bar{c}_{44}(1-\tilde{k}_e^2), \tag{A2}$$

and

$$\mathcal{T}_\pm(\zeta) := \exp\left[-\frac{1}{\pi}\int_{s_\ell}^{s_a}\arctan\left(\frac{-\tilde{k}_e^2\bar{\beta}(\eta)}{\alpha(\eta)}\right)\frac{d\eta}{\eta\pm\zeta}\right], \tag{A3}$$

where $\bar{\beta}(\eta):=\sqrt{\eta^2-s_\ell^2}$.

We first proceed to solve the stress-displacement Wiener-Hopf equation (44). Substituting Eq. (A1) into the Wiener-Hopf equation (58) yields

$$-D_s\frac{s_{bg}+\zeta}{\sqrt{s_a+\zeta}}\Delta U_+(\zeta)\mathcal{T}_+(\zeta)=\Sigma_-(\zeta)R_-(\zeta)+\frac{\sigma_0 g^*(p)R_-(\zeta)}{\zeta+s_h} \tag{A4}$$

where

$$R_-(\zeta) := \frac{\sqrt{s_a-\zeta}}{(s_{bg}-\zeta)\mathcal{T}_-(\zeta)} \tag{A5}$$

In order to separate the second term on the right side of Eq. (A4) into two sectionally analytic functions, additive factorization is performed. By inspection, a possible additive decomposition is

$$\frac{R_-(\zeta)}{\zeta+s_h}=\left(\frac{R_-(\zeta)-R_-(-s_h)}{\zeta+s_h}\right)_-+\left(\frac{R_-(-s_h)}{\zeta+s_h}\right)_+, \tag{A6}$$

where the constant $R_-(-s_h)$ is evaluated as

$$R_-(-s_h)=\frac{\sqrt{s_a+s_h}}{(s_{bg}+s_h)\mathcal{T}_-(-s_h)}. \tag{A7}$$

The Wiener-Hopf equation can then be rearranged into the desired form

$$-D_s\frac{s_{bg}+\zeta}{\sqrt{s_a+\zeta}}\Delta U_+(\zeta)\mathcal{T}_+(\zeta)-\frac{\sigma_0 g^*(p)R_-(-s_h)}{\zeta+s_h}=\Sigma_-(\zeta)R_-(\zeta)+\frac{\sigma_0 g^*(p)[R_-(\zeta)-R_-(-s_h)]}{\zeta+s_h}. \tag{A8}$$

Equating both left- and right-hand sides of (A8) to an entire function, say $ET(\zeta)$,

$$ET(\zeta)=\Sigma_-(\zeta)R_-(\zeta)+\frac{\sigma_0 g^*(p)(R_-(\zeta)-R_-(-s_h))}{\zeta+s_h} \tag{A9}$$

$$-ET(\zeta)=D_s\frac{s_{bg}+\zeta}{\sqrt{s_a+\zeta}}\Delta U_+(\zeta)\mathcal{T}_+(\zeta)+\frac{\sigma_0 g^*(p)R_-(-s_h)}{\zeta+s_h}. \tag{A10}$$

By the Abel theorem [41] and the extended Liouville's theorem [42], the entire function $ET(\zeta)$ must be identically zero. Hence,

$$\Sigma_-(\zeta)=\frac{\sigma_0 g^*(p)}{\zeta+s_h}\left(\frac{R_-(-s_h)}{R_-(\zeta)}-1\right) \tag{A11}$$

$$\Delta U_+(\zeta)=-\frac{\sigma_0 g^*(p)\sqrt{s_a+\zeta}R_-(-s_h)}{(\zeta+s_h)(s_{bg}+\zeta)D_s\mathcal{T}_+(\zeta)}. \tag{A12}$$

By substituting (A12) into Eqs. (53) and (54), one can obtain both $A_{sy}(\zeta)$ and $B_{sy}(\zeta)$,

$$A_{sy}(\zeta)=-\frac{\sigma_0 g^*(p)\sqrt{s_a+\zeta}R_-(-s_h)}{(\zeta+s_h)(s_{bg}+\zeta)D_s\mathcal{T}_+(\zeta)}, \tag{A13}$$

$$B_{sy}(\zeta)=\frac{e_{15}C_f\sigma_0 g^*(p)\sqrt{s_a+\zeta}R_-(-s_h)}{\epsilon_{11}(\zeta+s_h)(s_{bg}+\zeta)D_s\mathcal{T}_+(\zeta)}. \tag{A14}$$

The procedure of solving the electric potential-displacement Wiener-Hopf equation (59) is almost identical. Substituting Eq. (A1) into (59) yields

$$\frac{D_s(s_{bg}+\zeta)}{e_{15}^2(1-C_f)+\epsilon_{11}\tilde{c}_{44}}\frac{\Delta D_+(\zeta)\mathcal{T}_+(\zeta)}{(s_a+\zeta)\sqrt{s_\ell+\zeta}}=\Phi_-(\zeta)S_-(\zeta)+\frac{\phi_0 g^*(p)S_-(\zeta)}{\zeta+s_h} \tag{A15}$$

where

$$S_-(\zeta):=\frac{(s_a+\zeta)\sqrt{s_\ell+\zeta}}{(s_{bg}+\zeta)\mathcal{T}_-(\zeta)} \tag{A16}$$

By using the additive decomposition mentioned above, the Wiener-Hopf equation can then be rearranged into the desired form

$$\frac{D_s(s_{bg}+\zeta)}{e_{15}^2(1-C_f)+\epsilon_{11}\tilde{c}_{44}}\frac{\Delta D_+(\zeta)\mathcal{T}_+(\zeta)}{(s_a+\zeta)\sqrt{s_\ell+\zeta}}-\frac{\phi_0 g^*(p)S_-(-s_h)}{\zeta+s_h}$$
$$=\Phi_-(\zeta)S_-(\zeta)+\frac{\phi_0 g^*(p)[S_-(\zeta)-S_-(-s_h)]}{\zeta+s_h} \tag{A17}$$

where the constant $S_-(-s_h)$ is evaluated as

$$S_-(-s_h)=\frac{(s_a+s_h)\sqrt{s_\ell+s_h}}{(s_{bg}+s_h)\mathcal{T}_-(-s_h)}. \tag{A18}$$

Equating both the left- and right-hand sides of (A17) to an entire function, say $ET(\zeta)$,

$$ET(\zeta)=\Phi_-(\zeta)S_-(\zeta)+\frac{\phi_0 g^*(p)(S_-(\zeta)-S_-(-s_h))}{\zeta+s_h} \tag{A19}$$

$$ET(\zeta)=\frac{D_s(s_{bg}+\zeta)\Delta D_+(\zeta)\mathcal{T}_+(\zeta)}{[e_{15}^2(1-C_f)+\epsilon_{11}\tilde{c}_{44}](s_a+\zeta)\sqrt{s_\ell+\zeta}}-\frac{\phi_0 g^*(p)S_-(-s_h)}{\zeta+s_h}. \tag{A20}$$

Application of the Abel theorem [41] and the extended Liouville's theorem [42] reveals that the entire function $ET(\zeta)$ must be identically zero. Hence,

$$\Phi_-(\zeta)=\frac{\phi_0 g^*(p)}{\zeta+s_h}\left(\frac{S_-(-s_h)}{S_-(\zeta)}-1\right) \tag{A21}$$

$$\Delta D_+(\zeta)=-\frac{\phi_0 g^*(p)(s_a+\zeta)\sqrt{s_\ell+\zeta}S_-(-s_h)(e_{15}^2(1-C_f)+\epsilon_{11}\tilde{c}_{44})}{(\zeta+s_h)(s_{bg}+\zeta)\mathcal{T}_+(\zeta)D_s} \tag{A22}$$

The antisymmetry solution, $A_{an}(\zeta)$ and $B_{an}(\zeta)$, can then be obtained by substituting (A22) into Eqs. (56) and (57),

$$A_{an}(\zeta)=-\frac{\phi_0 g^*(p)\sqrt{s_a+\zeta}\sqrt{s_\ell+\zeta}S_-(-s_h)e_{15}}{\sqrt{s_a-\zeta}(s_{bg}+\zeta)\mathcal{T}_+(\zeta)D_s}, \tag{A23}$$

$$B_{an}(\zeta)=\frac{\phi_0 g^*(p)(s_a+\zeta)S_-(-s_h)\tilde{c}_{44}}{\sqrt{s_\ell-\zeta}(s_{bg}+\zeta)\mathcal{T}_+(\zeta)D_s}. \tag{A24}$$

References

[1] Auld, B. A., 1990, *Acoustic Fields and Waves in Solids*, 2nd ed., Krieger, Malabar, FL (two volumes).
[2] Berlincourt, D., 1981, "Piezoelectric Ceramics: Characteristics and Applications," J. Am. Ceram. Soc., **70**, pp. 1506–1595.
[3] Suo, Z., Kuo, C.-M., Barnett, D. M., and Willis, J. R., 1992, "Fracture Mechanics for Piezoelectric Ceramics," J. Mech. Phys. Solids, **40**, pp. 739–765.
[4] Cao, H. C., and Evans, A. G., 1994, "Electric-Field Induced Fatigue Crack Growth in Piezoelectrics," J. Am. Ceram. Soc., **77**, pp. 1783–1786.
[5] Culshaw, B., 1996, *Smart Structures and Materials*, Artech House, Boston.
[6] Uchino, K., 1998, "Materials Issues in Design and Performance of Piezoelectric Actuators: An Overview," Acta Mater., **46**, pp. 3745–3753.
[7] Shindo, Y., Togawa, R., and Moribayashi, H., 1999, "Scattering of Antiplane Shear Waves in a Piezoelectric Fibrous Composite Medium With Slip at Interfaces," J. Intell. Mater. Syst. Struct., **10**, pp. 257–262.
[8] Narita, F., and Shindo, Y. Y., 1999, "Scattering of Antiplane Shear Waves by a Finite Crack in Piezoelectric Laminates," Acta Mech., **134**, pp. 27–43.
[9] Wang, J., Sottos, N. R., and Weaver, R. L., 2003, "Mixed-Mode Failure of Thin Films Using Laser-Generated Shear Waves," Exp. Mech., **43**, pp. 323–330.
[10] Daros, C. H., and Antes, H., 2000, "The Elastic Motion of a Transversely Isotropic Piezoelectric Solid Caused by Impulsive Loading," ZAMP, **51**, pp. 397–418.
[11] Daros, C. H., and Antes, H., 2000, "On Strong Ellipticity Conditions for Piezoelectric Material of the Crystal Classes 6 mm and 622," Wave Motion, **31**, pp. 237–253.
[12] Li, S., 1996, "The Electromagneto-Acoustic Surface Wave in a Piezoelectric Medium: The Bleustein-Gulyaev Mode," J. Appl. Phys., **80**, pp. 5264–5269.
[13] Li, S., 2000, "Transient Wave Propagation in a Transversely Isotropic Piezoelectric Half Space," ZAMP, **51**, pp. 236–266.
[14] Daros, C. H., 2002, "A Fundamental Solutions for Transversely Isotropic, Piezoelectric Solids Under Electrically Irrotational Approximation," Mech. Res. Commun., **29**, pp. 61–71.
[15] Li, S., 2001, "On Diffraction in a Piezoelectric Medium by Half-Plane: The Sommerfeld Problem," ZAMP, **52**, pp. 101–134.
[16] Kottler, F., 1923, "Theory of Inflection in Black Screens," Ann. Phys., **70**, pp. 405–456.
[17] Kottler, F., 1965, "Diffraction at a Black Screen, Part I: Kirchoff Theory," Prog. Opt., **4**, pp. 281–314.
[18] Suo, Z., 1993, "Models for Breakdown-Resistant Dielectric and Ferroelectric Ceramics," J. Mech. Phys. Solids, **41**, pp. 1155–1176.
[19] Yang, W., and Suo, Z., 1994, "Cracking in Ceramic Actuators Caused by Electrostriction," J. Mech. Phys. Solids, **42**, pp. 649–663.
[20] Ru, C., 2000, "Electrode-Ceramic Interfacial Cracks in Piezoelectric Multilayer Materials," ASME J. Appl. Mech., **67**, pp. 255–261.
[21] Ru, C. Q., Mao, X., and Epstein, M., 1998, "Electric-Field Induced Interfacial Cracking in Multilayer Electrostrictive Actuators," J. Mech. Phys. Solids, **46**, pp. 1301–1318.
[22] Winzer, S. R., Shakar, N., and Ritter, A., 1989, "Designing Cofired Multilayer Electrostrictive Actuators for Reliability," J. Am. Ceram. Soc., **72**, pp. 2246–2257.
[23] Furuta, A., and Uchino, K., 1993, "Dynamic Observation of Crack Propagation in Piezoelectric Multilayer Ceramic Actuators," J. Am. Ceram. Soc., **76**, pp. 1615–1617.
[24] Aburatani, H., Harada, S., Uchino, K., and Furuta, A., 1994, "Destruction Mechanism of Ceramic Multilayer Actuators," Jpn. J. Appl. Phys., Part 1, **33**, pp. 3091–3094.
[25] Freiman, S. W., and White, G. S., 1994, "Intelligent Ceramic Materials: Issues of Brittle Fracture," in *Proceedings of the 2nd International Conference for Intelligent Materials*, Technical Publisher, Lancaster, PA, pp. 52–62.
[26] Hao, T. H., Gong, X., and Suo, Z., 1996, "Fracture Mechanics for the Design of Ceramic Multilayer Actuators," J. Mech. Phys. Solids, **44**, pp. 23–48.
[27] McMeeking, R. M., 1989, "On Mechanical Stresses at Cracks in Dielectrics With Application to Dielectric Breakdown," J. Appl. Phys., **62**, pp. 3116–3122.
[28] McMeeking, R. M., 1989, "Electrostrictive Stress Near Crack-Like Flaws," ZAMP, **40**, pp. 615–627.
[29] Fulton, C. C., and Gao, H., 2001, "Effect of Local Polarization Switching on Piezoelectric Fracture," J. Mech. Phys. Solids, **49**, pp. 927–952.
[30] Bleustein, J. L., 1968, "A New Surface Wave in Piezoelectric Materials," Appl. Phys. Lett., **13**, pp. 412–413.
[31] Gulyaev, Y. V., 1969, "Electrocoustic Surface Waves in Solids," Sov. Phys. JETP, **9**, pp. 37–38.
[32] Cagniard, L., 1939, *Reflexion et Refraction des Ondes Seismiques Progressives*. Gauthier-Villars, Paris. English translation; *Reflection and Refraction of Progressive Seismic Waves*, 1962, by E. A. Flinn and C. H. Dix, McGraw-Hill, New York.
[33] de Hoop, A. T., 1960, "A Modification of Cagniard's Method for Solving Seismic Pulse Problems," Appl. Sci. Res., Sect. B, **8**, pp. 349–360.
[34] Achenbach, J. D., 1973, *Wave Propagation in Elastic Solids*, North-Holland, Amsterdam.
[35] Liu, Y., Wang, C. H., and Ying, C. F., 1989, "Electromagnetic Acoustic Head Waves in Piezoelectric Media," J. Appl. Phys., **55**, pp. 434–436.
[36] Aki, K., and Richards, P. G., 2000, *Quantitative Seismology*, 2nd ed., University Science Books, Sausalito, CA.
[37] Freund, L. B., 1990, *Dynamic Fracture Mechanics*, Cambridge University Press, Cambridge.
[38] Sommerfeld, A., 1949, *Optics: Lectures on Theoretical Physics Vol. IV*, Academic Press, New York.
[39] Liu, Y., Wang, C. H., and Ying, C. F., 1995, "Head Waves in Piezoelectric Half Space," IEEE Trans. Ultrason. Ferroelectr. Freq. Control, **42**, pp. 66–72.
[40] Li, S., and Mataga, P. A., 1996, "Dynamic Crack Propagation in Piezoelectric Materials, Part I: Electrode Solution," J. Mech. Phys. Solids, **44**, pp. 1799–1830.
[41] van der Pol, B., and Bremer, H., 1955, *Operational Calculus*, 2nd ed., Cambridge University Press, Cambridge.
[42] Noble, B., 1958, *Methods Based on the Wiener-Hopf Technique*, Pergamon Press, New York.